Re-radiation Enhancement in Polarized Surface-Enhanced Resonant Raman Scattering of Randomly Oriented Molecules on Self-Organized Gold Nanowires

Barbara Fazio,[†] Cristiano D'Andrea,[†] Francesco Bonaccorso,[†,⊥] Alessia Irrera,[†] Giuseppe Calogero,[†] Cirino Vasi,[†] Pietro Giuseppe Gucciardi,[†,*] Maria Allegrini,[‡] Andrea Toma,[§,∥] Daniele Chiappe,[§] Christian Martella,[§] and Francesco Buatier de Mongeot[§]

[†]CNR IPCF Istituto per i Processi Chimico-Fisici, Viale F. Stagno D'Alcontres 37, I-98156, Messina, Italy, [‡]Dipartimento di Fisica "Enrico Fermi", Università di Pisa and INO-CNR Sezione di Pisa, Largo Bruno Pontecorvo 3, 56126 Pisa, Italy, and [§]Dipartimento di Fisica, Università di Genova, and CNISM, Via Dodecaneso 33, I-16146 Genova, Italy [⊥]Present address: Department of Engineering, University of Cambridge, Cambridge CB3 0FA, United Kingdom. [∥]Present address: Nanobiotech Facility, Istituto Italiano di Tecnologia, via Morego 30, Genova, I-16163, Italy.

ABSTRACT We explore the effect of re-radiation in surface-enhanced Raman scattering (SERS) through polarization-sensitive experiments on self-organized gold nanowires on which randomly oriented Methylene Blue molecules are adsorbed. We provide the exact laws ruling the polarized, unpolarized, and parallel- and cross-polarized SERS intensity as a function of the field polarizations. We show that SERS is polarized along the wire-to-wire nanocavity axis, independently from the excitation polarization. This proves the selective enhancement of the Raman dipole component parallel to the nanocavity at the single molecule level. Introducing a field enhancement tensor to account for the anisotropic polarization response of the nanowires, we work out a model that correctly predicts the experimental results for any excitation/detection polarization and goes beyond the E^4 approximation. We also show how polarization-sensitive SERS experiments permit one to evaluate independently the excitation and the re-radiation enhancement factors accessing the orientation-averaged non-diagonal components of the molecular Raman polarizability tensor.

KEYWORDS: nanoantennas · nanowires · self-organization · surface-enhanced Raman spectroscopy · polarization effects · field enhancement · Raman tensor

Optical nanoantennas (ONAs) such as metal nanowires (NWs), nanorods (NRs), and nanoparticles (NPs), both isolated and near-field coupled, offer new possibilities to focus and drive the optical fields at the nanometer scale.[1−6] ONAs permit enhancement of the absorption,[7] the fluorescence,[8,9] and the Raman scattering[10−12] of molecules and quantum emitters, as well as to control the light polarization[13−18] and the fluorescence emission direction.[16−18] The excitation of localized surface plasmon resonances (LSPRs) in ONAs is the basic mechanism for the giant signal amplification in surface-enhanced Raman scattering (SERS).[19−21] In SERS, the nanoantenna plays a two-fold role: on one hand, it amplifies the local field (excitation field enhancement), on the other, it magnifies the Raman scattering (re-radiation enhancement).[10,12] Molecules at the edges of individual ONAs[7,22,23] or in the nanocavities between near-field coupled NPs,[1,24−26] the so-called *hot spots*, experience an amplified local field and an enhanced scattering whenever both the laser pump (λ_L) and of the induced Raman dipole (λ_R) wavelengths are close to the LSPR one (λ_{LSP}).[21]

Polarization effects are at the center of ongoing research in the field of plasmonics and plasmon-enhanced spectroscopies.[13−17,27−29] In SERS, they provide new strategies to explore the field enhancement (FE) mechanisms and to probe the validity of the E^4 model,[30−33] which is the fundament of the current understanding of the SERS effect.[19−21] Field polarizations play a crucial role in anisotropic ONAs. In such systems, it is well-known that the enhanced local field is polarization-sensitive because the only component of the incident field exciting the LSPR and yielding the local field amplification is the one parallel to the nanoantenna axis.[34−37] On the other hand, the re-radiation effect is theoretically expected to selectively enhance only the component of the Raman dipole field parallel to the nanoantenna axis.[38] This implies that the SERS radiation should be linearly polarized. Such phenomenon can be experimentally proven in two ways. First by verifying that the intensity of the parallel- and cross-polarized SERS fields (with respect to the

* Address correspondence to gucciardi@me.cnr.it.

Received for review May 11, 2011 and accepted June 20, 2011.

Published online June 20, 2011
10.1021/nn201730k

excitation field) vary, respectively, as $I^{\parallel}_{SERS} \propto \cos^4\theta$ and $I^{\perp}_{SERS} \propto \cos^2\theta \times \sin^2\theta$ as a function of the angle θ between the excitation field polarization and the nanoantenna axis.[38] Second, by showing that the depolarization factor $D(\theta) = [I_{\parallel}(\theta) - I_{\perp}(\theta)]/[I_{\parallel}(\theta) + I_{\perp}(\theta)]$ satisfies the relation $D = \cos 2\theta$ with $D_{\theta=0} = +1$ and $D_{\theta=\pi/2} = -1$.[38] Reference 14 has demonstrated that SERS from a single molecule located in the nanocavity of a dimer is linearly polarized along the dimer axis, verifying the predicted angular relation for $D(\theta)$. The same authors[14,15] have shown that in trimers or tetramers the loss of axial symmetry, with respect to the dimer case, yields partially polarized SERS.[39,40]

Several issues on the re-radiation effect are, however, still unclear and remain the subject of active research. Indeed the $\cos^4\theta$ dependence for the cross-polarized intensity $I^{\perp}_{SERS}$, reported from single molecules in dimers,[41] is in disagreement with the theory.[38] The predicted $\cos^2\theta \times \sin^2\theta$ trend[38] has never been observed experimentally, up to date. The proof of this relation is of paramount importance in supporting the E^4 model, whose validity has been recently questioned.[30,32,33] SERS from randomly oriented molecules adsorbed on near-field-coupled NWs provides even more puzzling results. Indeed, contradictory $\cos^2\theta$ and $\cos^4\theta$ dependences for the unpolarized SERS intensity have been reported.[42−45] Moreover, it is unknown whether the SERS photons scattered by near-field-coupled NWs are polarized or not, and consequently, it is unclear if such systems actually behave as extended sets of dimers.[46] Whether SERS can be used to probe the Raman polarizability tensor of individual molecules is a further open question.[14,31,33,38,47] The SERS enhancement factor is known to be the product[21] $\Gamma_{SERRS} = |\Gamma_{exc}(\lambda_L)|^2 \times |\Gamma_{rad}(\lambda_R)|^2$ between the excitation, $\Gamma_{exc}(\lambda_L)$, and re-radiation, $\Gamma_{rad}(\lambda_R)$, FE factors. It remains, however, uncertain how to measure the two factors independently. Information on $\Gamma_{rad}(\lambda_R)$ and $\Gamma_{exc}(\lambda_L)$ is crucial because it permits one to gain insight on the spectral dependence of the SERS enhancement[32,48,49] and to validate the proportionality relation between the FE factors and the LSPR extinction intensity,[32,50] especially in the presence of multipolar[51] and Fano resonances.[52] All of these aspects have, in addition, a strong applicative relevance. Information on the wavelength dependence and polarization properties of SERS signal, in fact, allow for the optimization of SERS molecular sensors, defining the best excitation/detection wavelengths[35,53] and field polarization orientations[54,55] for maximum signal enhancement and background rejection.

The aim of this article is to shed light on the aforementioned issues. This is done through a systematic study of the polarized SERS from randomly oriented molecules adsorbed on self-organized gold NW arrays. We experimentally investigate the polarization state of the SERS photons for different excitation polarizations showing the exact dependence of parallel-polarized, cross-polarized, and unpolarized SERS intensities as a function of the relative orientation between the NWs and the excitation field. We develop a phenomenological model, introducing a FE tensor to describe the anisotropic response of the NWs and accounting for the incoherent SERS scattering of different molecules. We find that dealing with many randomly oriented molecules greatly simplifies the calculations, allowing us to derive simple relations able to correctly interpret the experimental findings and, at the same time, to estimate the excitation and the re-radiation FE factors, independently, from a fit of the experimental data. Furthermore, this approach permits one to gain information on the orientation-averaged non-diagonal components of the Raman tensor of the probe molecule. Finally, the E^4 model and the related approximations are critically analyzed and discussed.

RESULTS AND DISCUSSION

Morphology Analysis and Plasmon Resonance. Experiments are carried out on a novel kind of SERS-active substrate based on a dense array of self-organized AuNWs supported on glass substrates, formed through ion beam sputtering (IBS).[56,57] The process was optimised in order to tailor the anisotropic plasmonic response of the NWs[58] (see Methods and Supporting Information, section 1). Figure 1a displays the topography measured by atomic force microscopy (AFM) of a disconnected gold film, yielding an array of adjacent NWs after an irradiation dose of 3.96×10^{18} ions/cm^2 (further images are reported in Figure S1). The elongation of the NWs parallel to the projection of the ion beam can easily exceed 3 μm, irrespective of the average grain size, which is in the order of 100 nm. The average NWs periodicity $\Lambda = (130 \pm 10)$ nm is derived from the 2D fast Fourier transform of the AFM images, after differential filtering to enhance the ripple contrast. Figure 1b shows the polarized optical transmission spectra. No LSPRs are present in the visible range for light polarized along the NWs long axis $\hat{\mathbf{n}}_y$ (Figure 1b, black line). Conversely, a broad LSPR peak appears around 700 nm (Figure 1b, yellow line) for excitation polarized parallel to the NW's short axis $\hat{\mathbf{n}}_x$ (coincident with the wire-to-wire nanocavity axis). Quasi-static Mie approximation calculations permit explanation of the LSPR broadening in terms of inhomogeneous broadening due to the spread in the geometrical parameters of the NWs.[58] Both the laser wavelength used for SERS excitation (633 nm, red vertical line in Figure 1b) and the Raman scattering wavelengths of the probe molecules (650−705 nm, violet box in Figure 1b) are resonant with the LSPR of the NWs. The transmission is lower (*i.e.*, extinction is higher) at the Raman scattering energy (Figure 1c, filled circles) than at the laser energy (Figure 1c, open diamonds). The transmission (Figure 1c, hollow red diamonds) depends on the angle, θ, between the incident field polarization vector $\hat{\mathbf{e}}_{exc}$ and the axis

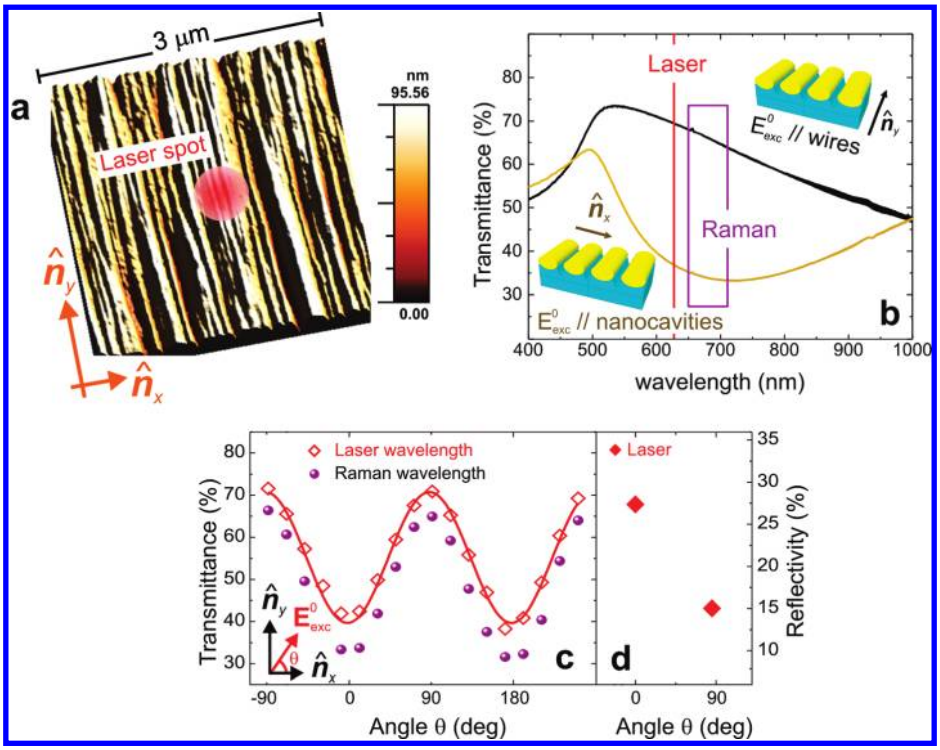

Figure 1. (a) AFM topography of the gold nanowire sample ($3 \times 3\ \mu m^2$). The laser irradiated area (*ca.* 600 nm diameter) is indicated by the red spot. (b) Transmission spectra with excitation polarized parallel to the nanowires long axis $\hat{n}_y$ (black line) or parallel to the wire-to-wire nanocavities axis $\hat{n}_x$ (yellow line). The red line indicates the spectral position of the 633 nm laser line used for SERS; the violet box indicates the spectral range of the Raman scattering of MB molecules. (c) Sample transmittance at the laser (hollow red diamonds) and at the Raman wavelengths (violet solid circles) as a function of the angle θ between the light polarization vector $\hat{e}_{exc}$ and the wire-to-wire nanocavity axis $\hat{n}_x$. The red line is a fit of the transmittance using a $T_0(1 - A\cos^2\theta)$ model. (d) Sample reflectivity is higher (27%) for the field component along the nanocavity axis than for the one parallel to the nanowires long axis (15%).

$\hat{n}_x$, as $T(\theta) = T_0(1 - A\cos^2\theta)$ as highlighted by the fit (Figure 1c, red line). This behavior suggests that only the field component parallel to $\hat{n}_x$ ($|\vec{E}_{exc} \cdot \hat{n}_x| \propto \cos\theta$) contributes to the LSPR excitation.[35,44,45] The sample reflectivity at 633 nm, measured as the ratio between the reflected and the incident field intensities, is about two times higher for light polarized along $\hat{n}_x$ (Figure 1d, $\theta = 0°$) than for light polarized along $\hat{n}_y$ ($\theta = 90°$), that is, $R_{\hat{n}_x}/R_{\hat{n}_y} \approx 2$. The dichroic behavior of the sample occurs only for ion doses sufficient to disconnect the NWs array. For a reduced ion dose and a still connected film, the transmission spectra resemble closely those measured for polarization parallel to $\hat{n}_y$ (Figure 1b, black line).[56] This result confirms that the 700 nm band is due to the spatial localization of surface plasmons along the NWs short axis and at the wire-to-wire nanocavities. Theoretical calculations[26] and experimental observations[1] suggest that the optical field enhancement at the nanocavity of near-field-coupled nanostructures is orders of magnitude more intense with respect to that observed on individual nanostructures. Since the SERS enhancement scales as the fourth power of the FE factor, we expect that most of the contribution to our SERS signal arises from molecules in the *hot spots* located in the nanocavities between adjacent NWs, although we cannot exclude a contribution from the resonant excitation of the LSPRs along the NW's short axis.[59,60]

Polarized SERRS. Surface-enhanced resonant Raman scattering (SERRS) and polarization-sensitive SERRS (pSERRS) experiments are carried out using Methylene Blue (MB) as molecular probe. MB is pre-resonantly excited at 633 nm (Figure S2). Resonant excitation gives a further boost to the Raman scattering[61] permitting one to record a measurable signal even in the absence of plasmonic enhancement. MB has been bound to the NWs by immersing the glass substrate in a deionized aqueous solution at 3×10^{-4} M concentration for 1 h (see Supporting Information section 2 for further details). The sample is subsequently rinsed repeatedly in deionized water in order to remove the MB excess, leaving a monolayer of molecules on the NWs surface.[60] Scanning tunneling microscopy measurements show that MB adsorbs on gold by forming nanometer scale random patches.[62] pSERRS measurements are performed in backscattering, exciting with a linearly polarized laser at 633 nm (Figure 2). The incident polarization, $\hat{e}_{exc}$, is rotated by an angle θ relative to the nanocavities axis $\hat{n}_x$ (Figure 2, red inset). A polarizer is used to analyze the $\hat{e}_{det}$ component of the Raman field polarized at an angle ϕ with respect to the incident field $\hat{e}_{exc}$ (Figure 2, green inset). More details

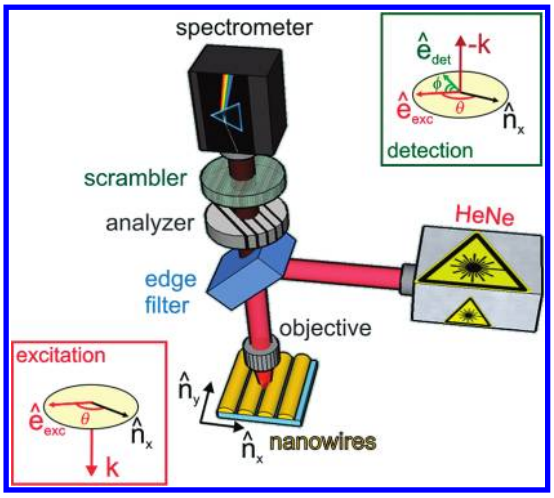

Figure 2. Sketch of the setup for polarized SERRS. Experiments are carried out on a Jobin-Yvon HR800 spectrometer working in backscattering mode. The laser excitation (633 nm) is linearly polarized and focused on the sample with a 100× objective. The laser field $\hat{e}_{exc}$ is linearly polarized at an angle θ with respect to the nanocavity axis $\hat{n}_x$ (red inset). The sample is rotated underneath the objective to change θ. The backscattered radiation is collected through the same objective, and a polarization analyzer with optical axis $\hat{e}_{det}$ oriented at an angle ϕ with respect to the excitation field $\hat{e}_{exc}$ (green inset) is used to acquire the polarized SERRS signal.

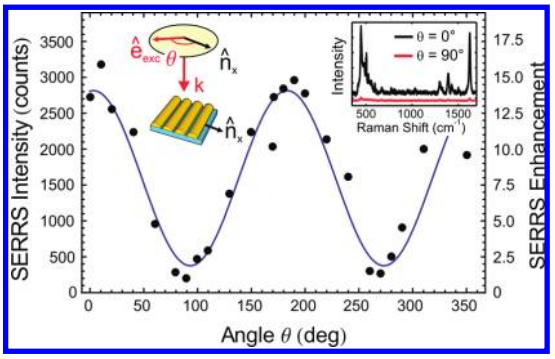

Figure 3. (black symbols) Unpolarized SERRS intensity versus excitation polarization θ. SERRS is maximum for $\theta = 0°$ (inset, black line), *i.e.* for $\hat{e}_{exc}$ parallel to the nanocavity axis $\hat{n}_x$, and minimum for $\theta = 90°$ (inset, red line), *i.e.* $\hat{e}_{exc}$ parallel to NWs long axis $\hat{n}_y$. $I^{unpol}_{SERRS}(\theta)$ is well fitted with a law $|\Gamma_{exc} \times \Gamma_{rad}|^2 \times \cos^2\theta$ (blue line), plus lower order terms. The SERRS enhancement is calculated by normalizing the intensity to its minimum value, *i.e.* for $\hat{e}_{exc} \perp \hat{n}_x$.

can be found in the Methods section. MB has intense Raman-active vibrations in the 400−1630 cm^{-1} range (Figure S3a).[63] The pSERRS analysis hereafter refers to the C−N−C skeleton bending mode at 446 cm^{-1} which is red-shifted by 20 nm with respect to the laser pump and whose intensity ratio with the adjacent peak at 470 cm^{-1} gives indications of the chemical state of the MB molecules (see Supporting Information, section 3.2). We assume the signal intensity, I, as the peak intensity after subtraction of the continuum background.[64] The depolarization ratio[61] is calculated as $\rho = I_\perp/I_\parallel$ where $I_\perp$ is the intensity of Raman scattering component polarized orthogonally to the excitation and $I_\parallel$ is the one polarized parallel to it. Depolarization ratios have been exploited in SERS to highlight the polarization rotation occurring in nanoparticle aggregates[14,15] and nanoellipsoids.[32] Here we use ρ to highlight the polarization rotation induced by NWs, with respect to SERS from gold NPs and MB molecules cast on glass. Resonant Raman spectra (RRS) of randomly oriented molecules cast on a glass substrate show that the Raman scattering from MB is partially polarized (Figure S3a). The depolarization ratio of the 446 cm^{-1} mode is $\rho = I_\perp/I_\parallel = 0.50 \pm 0.03$ (Figure S3b). When MB is adsorbed on a SERS-active substrate consisting of near-field-coupled gold NPs (inset of Figure S4) optically resonant at 633 nm (Figure S4), the depolarization ratio decreases to $\rho = I_\perp/I_\parallel \cong 0.34 \pm 0.02$ (Figure S5), as expected for SERS from a set of randomly oriented nanocavities.[33]

In NWs the sample's anisotropy makes the SERS intensity a function of both the excitation polarization angle and the analyzer orientation, that is, $I_{SERRS} = I_{SERRS}(\theta,\phi)$. To gain insight on the polarization dependence of both the SERS and the local excitation field, we have carried out three different experiments:

1. Study of the total unpolarized SERRS intensity, $I^{unpol}_{SERRS}(\theta) = I^{\parallel}_{SERRS}(\theta) + I^{\perp}_{SERRS}(\theta)$ *versus* the excitation polarization angle ($\theta = 0°,...,360°$).
2. Analysis of the pSERRS intensity $I_{SERRS}(\phi)|_{\bar{\theta}=0°,90°,150°}$ as a function of the analyzer angle ($\phi = 0°,...,360°$) for three different excitation polarizations $\bar{\theta} = 0$, 90, and 150°.
3. Analysis of the parallel- and cross-polarized intensities of the SERRS field, $I^{\parallel}_{SERRS}(\theta) = I_{SERRS}(\theta)|_{\phi=0°}$ and $I^{\perp}_{SERRS}(\theta) = I_{SERRS}(\theta)|_{\phi=90°}$, as a function of the excitation polarization ($\theta = 0°,...,360°$).

The unpolarized SERRS intensity strongly varies with the excitation polarization angle θ (Figure 3, black symbols and Figure S6 in the Supporting Information), highlighting the anisotropic FE properties of the sample. The SERRS spectra for excitation polarization parallel ($\theta = 0°$, black line) and orthogonal to $\hat{n}_x$ ($\theta = 90°$, red line) are reported in the inset of Figure 3. SERRS is maximum for excitation polarization parallel to the nanocavity axis $\hat{n}_x$ and minimum for polarization along the nanowires long axis $\hat{n}_y$. The SERRS signal enhancement (*i.e.*, max-to-min ratio) is here *ca.* 15. The experimental data are well fitted by a law $I^{unpol}_{SERRS}(\theta) \sim |\Gamma_{exc} \times \Gamma_{rad}|^2 \times \cos^2\theta$ (Figure 3, blue line). The $\cos^2\theta$ behavior confirms that only the laser field component parallel to nanocavities' axis $\hat{n}_x$, that is, $\vec{E}_{eff} \propto (\hat{e}_{exc} \cdot \hat{n}_x)\hat{n}_x = (\cos\theta)\hat{n}_x$ contributes to the SERS enhancement.

The polarization properties of the enhanced Raman field are usually studied through the depolarization factor $D(\theta) = [I_\parallel(\theta) - I_\perp(\theta)]/[I_\parallel(\theta) + I_\perp(\theta)]$.[14,15,39,40] Differently, here we carry out a direct analysis of the SERS field

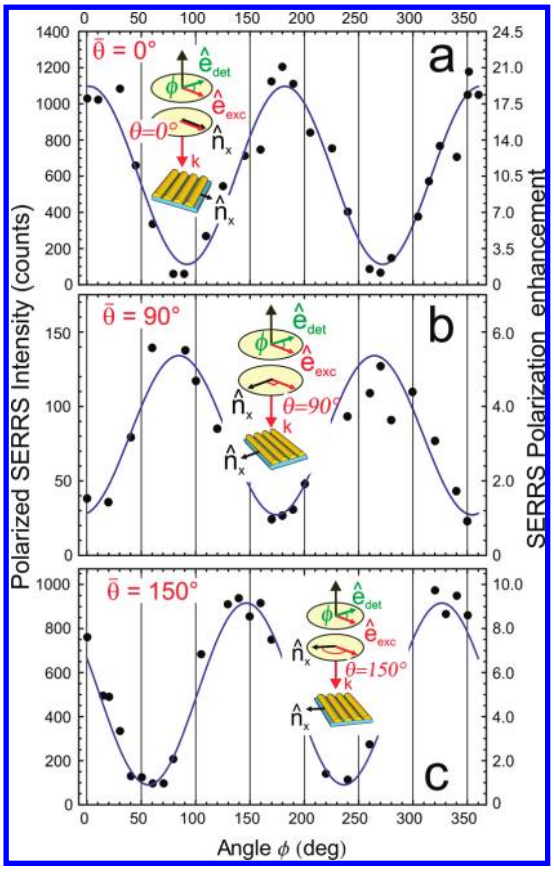

Figure 4. Polarized SERRS intensities (black symbols) measured for incident polarization (a) parallel to the nanocavity axis $\hat{n}_x$ ($\bar{\theta} = 0°$), (b) orthogonal to $\hat{n}_x$ ($\bar{\theta} = 90°$), and (c) at an angle $\bar{\theta} = 150°$ with respect to $\hat{n}_x$. The SERRS signal is always maximum when the analyzer is oriented parallel to the nanocavity axis $\hat{n}_x$, no matter the orientation, $\bar{\theta}$, of the excitation polarization. $I_{SERRS}(\phi)$ is well fitted by a law $|\Gamma_{exc} \times \Gamma_{rad}|^2 \times \cos^2(\phi - \bar{\theta})$ (blue lines), plus lower order terms. In each experiment, the SERRS polarization enhancements are calculated by normalizing to the minimum signal value.

polarization by means of a rotating analyzer to visualize the polarization state of scattered photons and check for polarization rotations induced by the re-radiation effect. We excite the NWs with a laser field $\hat{\mathbf{e}}_{exc}$ polarized along three different directions with respect to $\hat{\mathbf{n}}_x$, namely, $\bar{\theta} = 0$, 90, and 150°, and we analyze for each $\bar{\theta}$ the intensity of the SERRS component polarized along $\hat{\mathbf{e}}_{det}$ at an angle ϕ with respect to the laser field $\hat{\mathbf{e}}_{exc}$ (as depicted in the sketches of Figure 4 and in Figure S10 in the Supporting Information). For $\hat{\mathbf{e}}_{exc}$ parallel to the nanocavity axis ($\bar{\theta} = 0°$), the SERRS is polarized along the same direction $\hat{\mathbf{n}}_x$ (Figure 4a and Figure S7a). $I_{SERRS}(\phi)$ is maximum for $\phi = 0°,180°$ and minimum for $\phi = 90°,270°$. The maximum-to-minimum intensity ratio, defined hereafter as the SERRS polarization enhancement, is ~20. Rotating $\hat{\mathbf{e}}_{exc}$ by 90°, orthogonal to the nanocavity axis $\hat{\mathbf{n}}_x$, we find (Figure 4b and Figure S7b) that the SERRS is still maximum in the nanocavity axis direction $\hat{\mathbf{n}}_x$ ($\phi = 90°,270°$) and minimum along the laser polarization direction ($\phi = 0°,180°$). This indicates that we are facing a complete 90° polarization rotation with respect to the laser field. The SERRS polarization enhancement here is ~5.6. We have finally chosen an excitation polarization angle $\bar{\theta} = 150°$ that breaks the sample's symmetry. Again, we find that the SERRS is polarized along the nanocavity axis $\hat{\mathbf{n}}_x$ (Figure 4c and Figure S7c) with a 150° polarization rotation with respect to the laser field. Here the SERRS polarization enhancement is ~9. The polar plots in Figure S7 give a bird's eye view of the SERRS polarization rotation when turning the sample under the laser field. The experimental data are well fitted by a law $I_{SERRS}(\phi) \sim \cos^2(\phi - \bar{\theta})$. Note that ρ for the 446 cm^{-1} mode ($\rho = I_\perp/I_\parallel$, where $I_\perp$ and $I_\parallel$ refer to the laser polarization orientation) is now dependent on the laser polarization angle θ, with values $\rho_{SERRS}|_{\bar{\theta}=0°} \approx 1/20$, $\rho_{SERRS}|_{\bar{\theta}=90°} \approx 5$, $\rho_{SERRS}|_{\bar{\theta}=150°} \approx 1/2$. Notably, for $\bar{\theta} = 90°$, the depolarization ratio is *ca.* 10 times higher than the value measured on glass and *ca.* 7 times larger than the maximum theoretical value[61] of 0.75 (see Supporting Information, section 3.5). This result confirms that the NWs are strongly polarizing the Raman scattering and that the θ dependence of the depolarization ratios is due to the strong coupling of the laser with the anisotropic LSPR of the NWs and is not related to the molecular orientation or to the MB Raman tensor. Furthermore, the numerical values $\rho_{SERRS}|_{\bar{\theta}=90°} \approx 5$ and $\rho_{SERRS}|_{\bar{\theta}=0°} \approx 1/20$ confirm that this phenomenon is a near-field re-radiation effect and is not caused by the sample far-field dichroism. In the latter case, in fact, considering that the dichroic reflectivity ratio of the sample is $R_{\hat{\mathbf{n}}_x}/R_{\hat{\mathbf{n}}_y} \approx 2$, and that the depolarization ratio of MB molecules is $\rho \cong 1/2$, we would have expected values $\rho_{SERRS}|_{\bar{\theta}=0°} \approx R_{\hat{\mathbf{n}}_x}/R_{\hat{\mathbf{n}}_y} \times \rho \approx 1$ and $\rho|_{\bar{\theta}=0°} = R_{\hat{\mathbf{n}}_y}/R_{\hat{\mathbf{n}}_x} \times \rho \approx 1/4$, different from our experimental findings.

We have finally analyzed the angular dependence of the parallel- and the cross-polarized SERRS intensities, $I^{\parallel}_{SERRS}(\theta)$ and $I^{\perp}_{SERRS}(\theta)$. Results are shown in Figure 5 (red and blue symbols, respectively) and in the polar plots of Figure S8. We note that $I^{\parallel}_{SERRS} \sim \cos^4\theta$ (red line), with maxima for $\hat{\mathbf{e}}_{exc} \parallel \hat{\mathbf{n}}_x$ ($\theta = 0°,180°$) and minima for $\hat{\mathbf{e}}_{exc} \perp \hat{\mathbf{n}}_x$ ($\theta = 90°,270°$), while the cross-polarized SERRS intensity follows a law $I^{\perp}_{SERRS} \sim \cos^2\theta \times \sin^2\theta$ (blue line) with minima for $\theta_n = n \times 90°$ and maxima for $\theta_n = 45° + n \times 90°$ (n is an integer). Notably, the minima do not have equal intensity. $I^{\perp}_{SERRS}|_{\theta=90°,270°}$ is more intense than $I^{\perp}_{SERRS}|_{\theta=0°,180°}$, as shown more clearly in the inset of Figure 5. Systematic measurements on 18 different sample points (Figure S9) confirm this trend and provide a precise estimate of the ratio $\Delta = I^{\perp}_{SERRS}|_{\theta=90°}/I^{\perp}_{SERRS}|_{\theta=0°} = 1.5 \pm 0.3$. To rule out any possible depolarization effect in the excitation field,[65] measurements have been carried out using a 20× long working distance microscope objective with NA 0.25.

The experimental proof of the relations $I^{\parallel}_{SERRS} \sim \cos^4\theta$ and $I^{\perp}_{SERRS} \sim \cos^2\theta \times \sin^2\theta$ represents the first full confirmation of the theoretical predictions based on the E^4 model[38] and validates the hypothesis according to which near-field-coupled NWs behave as extended

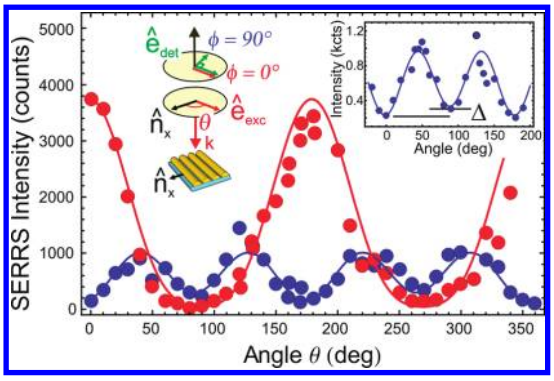

Figure 5. Plot of the parallel- (red symbols) and cross-polarized (blue symbols) SERRS intensity *vs* the excitation polarization angle θ. The parallel-polarized component is well fitted (red line) by a law $I^{\parallel}_{SERRS} \sim |\Gamma_{exc} \times \Gamma_{rad}|^2 \times \cos^4\theta$, plus lower order terms. The cross-polarized component depends on θ as $I^{\perp}_{SERRS} \sim \cos^2\theta \times \sin^2\theta$ (blue line). The latter is only an approximation since, as highlighted in the inset (blue symbols), $I^{\perp}_{SERRS}|_{\theta=0^\circ} \neq I^{\perp}_{SERRS}|_{\theta=90^\circ}$ with a ratio $\Delta = 1.5$ between two consecutive minima.

dimers. From the physical point of view, these relations are straightforward consequences of the polarized nature of the SERRS radiation. New insight can be retrieved by a careful analysis of the physical information encoded in $I^{\parallel}_{SERRS}(\theta)$ and $I^{\perp}_{SERRS}(\theta)$ calculated at $\theta = 0$ and 90°. $I^{\parallel}_{SERRS}|_{\theta=0^\circ}$ is the SERRS intensity measured exciting with a field $\hat{\mathbf{e}}_{exc} \parallel \hat{\mathbf{n}}_x$ (yielding maximum enhancement of the local field) and probing the Raman component $\hat{\mathbf{e}}_{det} \parallel \hat{\mathbf{n}}_x$ (which experiences maximum re-radiation enhancement). $I^{\parallel}_{SERRS}|_{\theta=90^\circ}$ is the signal measured in the absence of any enhancement since both fields $\hat{\mathbf{e}}_{exc}$ and $\hat{\mathbf{e}}_{det}$ are orthogonal to $\hat{\mathbf{n}}_x$. The ratio $I^{\parallel}_{SERRS}|_{\theta=0^\circ}/I^{\parallel}_{SERRS}|_{\theta=90^\circ}$ is therefore expected to be equal to the SERRS enhancement factor $\Gamma_{SERRS} = |\Gamma_{exc}(\lambda_L)|^2 \times |\Gamma_{rad}(\lambda_R)|^2$. In our case, we measure $\Gamma_{SERRS} \sim 40$ (Figure S8a). Concerning the cross-polarized component, $I^{\perp}_{SERRS}|_{\theta=0^\circ}$ is the signal measured in conditions of maximum local field enhancement ($\hat{\mathbf{e}}_{exc} \parallel \hat{\mathbf{n}}_x$) and null re-radiation enhancement (we detect the Raman component $\hat{\mathbf{e}}_{det} \perp \hat{\mathbf{n}}_x$). Conversely, $I^{\perp}_{SERRS}|_{\theta=90^\circ}$ is the signal measured in conditions of null local field enhancement ($\hat{\mathbf{e}}_{exc} \perp \hat{\mathbf{n}}_x$) and maximum re-radiation enhancement (the Raman component $\hat{\mathbf{e}}_{det} \parallel \hat{\mathbf{n}}_x$ is detected). We therefore expect that the ratio $\Delta = I^{\perp}_{SERRS}|_{\theta=90^\circ}/I^{\perp}_{SERRS}|_{\theta=0^\circ}$ is equal to the ratio $|\Gamma_{rad}(\lambda_R)|^2/|\Gamma_{exc}(\lambda_L)|^2$. Since $\lambda_R > \lambda_L$, the ratio Δ can be different from 1 due to the spectral dependence of the enhancement factors.[48] Our experiments show that $\Delta = 1.5$, that is, $\Gamma_{rad}(\lambda_R) > \Gamma_{exc}(\lambda_L)$ and are in agreement with the higher extinction (lower transmission in Figure 1b) measured at the Raman scattering wavelength with respect to the excitation one.

Modeling of Polarized SERS. To better understand these results, we model the electromagnetic (EM) SERS enhancement by extending previous calculations on polarized SERS from single molecules in dimers[12,14,15,38] to the case of many randomly oriented molecules adsorbed on aligned NWs (further details are given in the Methods section). A molecule located at the *hot spot* of a nanoantenna optically resonant at λ_{LSP} experiences a local excitation field $\vec{\mathbf{E}}^{enh}_{exc}(\lambda_L) = \Gamma_{exc}(\lambda_L)\vec{\mathbf{E}}^{0}_{exc}(\lambda_L)$ strongly enhanced with respect to the pump $\vec{\mathbf{E}}^{0}_{exc}(\lambda_L)$ whenever $\lambda_L \approx \lambda_{LSP}$. This induces a Raman dipolar field $\vec{\boldsymbol{\mu}}^{0}_{rad}(\lambda_R) = \vec{\boldsymbol{\alpha}} \cdot \vec{\mathbf{E}}^{enh}_{exc}(\lambda_L)$ ($\vec{\boldsymbol{\alpha}}$ is the polarizability tensor of the Raman mode) radiating at wavelength λ_R. If also $\lambda_R \approx \lambda_{LSP}$, the scattered field is, in turn, further amplified by the re-radiation effect, providing an enhanced Raman field $\vec{\boldsymbol{\mu}}^{enh}_{rad}(\lambda_R) = \Gamma_{rad}(\lambda_R)\vec{\boldsymbol{\mu}}^{0}_{rad}(\lambda_R)$. If the nanoantenna is isotropic, we can assume both the enhancement factors, $\Gamma_{exc}(\lambda_L)$ and $\Gamma_{rad}(\lambda_R)$, to be scalar multiplicative constants. In anisotropic ONAs, such as NRs, NWs, or dimers, we can introduce a field enhancement tensor $\vec{\vec{\Gamma}}(\lambda)$[14] to describe the anisotropic optical amplification, yielding the expressions $\vec{\mathbf{E}}^{enh}_{exc}(\lambda_L) = \vec{\vec{\Gamma}}_{exc}(\lambda_L) \cdot \vec{\mathbf{E}}^{0}_{exc}(\lambda_L)$ and $\vec{\boldsymbol{\mu}}^{enh}_{rad}(\lambda_R) = \vec{\vec{\Gamma}}_{rad}(\lambda_R) \cdot \vec{\boldsymbol{\mu}}^{0}_{rad}(\lambda_R)$ for the enhanced fields. Our NWs feature a single resonance λ^{x}_{LSP} in the visible range along the wire-to-wire nanocavity axis $\hat{\mathbf{n}}_x$. We therefore introduce the FE tensors

$$\vec{\vec{\Gamma}}_{exc}(\lambda_L \approx \lambda^{x}_{LSP}) = \begin{pmatrix} \Gamma & 0 & 0 \\ 0 & 1 & 0 \\ 0 & 0 & 1 \end{pmatrix}$$
$$\vec{\vec{\Gamma}}_{rad}(\lambda_R \approx \lambda^{x}_{LSP}) = \begin{pmatrix} \Gamma(1+\varepsilon) & 0 & 0 \\ 0 & 1 & 0 \\ 0 & 0 & 1 \end{pmatrix} \quad (1)$$

to model the fact that NWs enhance the field components parallel to the nanocavity axis $\hat{\mathbf{n}}_x$, leaving the component along $\hat{\mathbf{n}}_y$ unperturbed. The form of the FE tensors in eq 1 is notably different from the one assumed in ref 14, referred to trimers. The factor $(1 + \varepsilon)$ accounts for the wavelength dependence of the enhancement factors,[49] assuming different excitation, $\Gamma_{exc}(\lambda_L) = \Gamma$, and re-radiation, $\Gamma_{rad}(\lambda_R) = \Gamma(1 + \varepsilon)$, amplification factors. For a single molecule, the SERS intensity is given by $I_{SERS} = |\hat{\mathbf{e}}_{det} \cdot \vec{\boldsymbol{\mu}}^{enh}_{rad}|^2$. In the case of N randomly oriented molecules, the SERS signal is the sum of the incoherent scattering of each molecule, averaged over all the possible molecular orientations, that is

$$I_{SERS} \propto N\left\langle |\hat{e}_{det} \cdot \vec{\vec{\Gamma}}_{rad}(\lambda_R) \cdot \vec{\vec{\alpha}}(\xi, \zeta, \psi) \cdot \vec{\vec{\Gamma}}_{exc}(\lambda_L) \cdot \hat{e}_{exc}|^2 \right\rangle_{\xi, \zeta, \psi} \quad (2)$$

where ξ,ζ,ψ are the Euler angles of the molecule (see Methods). Assuming a generic form for the Raman tensor $\vec{\vec{\alpha}}$, the expression of the pSERRS intensity in the backscattering configuration for generic polarization angles (θ,ϕ) results as

$$\begin{aligned} I_{SERS}(\theta,\phi) \propto\ & \Gamma^4(1+\varepsilon)^2 \times \langle\alpha^2_{ii}\rangle \times [\cos^2\theta \times \cos^2(\theta-\phi)] \\ & + \Gamma^2(1+\varepsilon) \times \langle\alpha^2_{ii}\rangle \times [1/2 \times \sin 2\theta \times \sin 2(\theta-\phi)] \\ & + \Gamma^2 \times \langle\alpha^2_{ij}\rangle \times [\varepsilon \times \cos(\theta-\phi) \times \sin\theta + \sin\phi]^2 \\ & + \langle\alpha^2_{ii}\rangle \times [\sin^2\theta \times \sin^2(\theta-\phi)] \end{aligned} \quad (3)$$

where $\langle\alpha_{ii}^2\rangle$ and $\langle\alpha_{ij}^2\rangle$ are the orientation averaged diagonal and off-diagonal elements of the Raman polarizability tensor.[61] $I_{SERS}(\theta,\phi)$ is the sum of four terms. Each one is the product of a FE, a Raman polarizability and a geometric factor (in square brackets). The geometric factors describe the polarization dependence of I_{SERS}. For large FE factors ($\Gamma^4 \gg \Gamma^2 \gg 1$), the first term of the order of Γ^4 rules

$$I_{SERS}(\theta,\phi) \propto \Gamma^4(1+\varepsilon)^2 \times \langle\alpha_{ii}^2\rangle \times [\cos^2\theta \times \cos^2(\theta-\phi)] \quad (4)$$

Equation 4 shows that the polarization dependence in SERS is described by the law $\cos^2\theta \times \cos^2(\theta-\phi)$. This term correctly predicts the angular dependence for the polarized $\sim \cos^2(\phi-\bar{\theta})$, unpolarized $\sim \cos^2\theta$, parallel-polarized $\sim \cos^4\theta$, and cross-polarized $\sim \cos^2\theta \cdot \sin^2\theta$ intensities, as well as for the depolarization factor, $D \sim \cos 2\theta$. For what concerns the enhancement factor, equation 4 gives an expression identical to the one derived from the E^4 model, *i.e.* $\Gamma_{SERRS} = \Gamma^4(1+\varepsilon)^2 = \Gamma^2_{exc}(\lambda_L) \times \Gamma^2_{rad}(\lambda_R)$, and shows that for $\Gamma^2_{exc}(\lambda_L) \approx \Gamma^2_{rad}(\lambda_R)$ ($\varepsilon = 0$ in our formalism), the SERS enhancement scales as Γ^4, *i.e.* the fourth power of the FE factor. Equation 4 carries information only on $\langle\alpha_{ii}^2\rangle$, and this explains why it cannot be used to gain information on the Raman polarizability tensor. The two terms of order Γ^2 in eq 3 are beyond the E^4 approximation. These terms bring a weaker contribution to the SERRS signal, of the order of $\sim 1/\Gamma^2$ with respect to the first one, but they carry information on both $\langle\alpha_{ii}^2\rangle$ and $\langle\alpha_{ij}^2\rangle$ and therefore give information on the Raman polarizability tensor of the probe molecule. In particular, they permit one to measure the depolarization ratio $\rho = \langle\alpha_{ij}^2\rangle/\langle\alpha_{ii}^2\rangle$ of the molecular vibrations. The last term in eq 3 yields an even smaller contribution to the SERRS signal ($\sim 1/\Gamma^4$). However, the ability to probe experimentally this term is important since it is related to the Raman signal measured in the absence of any enhancement and, therefore, can be used as a reference to precisely evaluate the SERRS enhancement.

The expressions for the different pSERRS signals are obtained from eq 3. For the parallel- and cross-polarized intensities, we find

$$I^{\parallel}_{SERRS}(\theta) \propto \Gamma^4(1+\varepsilon)^2 \times \langle\alpha_{ii}^2\rangle \times \cos^4\theta + \Gamma^2[\langle\alpha_{ij}^2\rangle \times \varepsilon^2 + 2 \times \langle\alpha_{ii}^2\rangle \times (1+\varepsilon)] \times [\cos^2\theta \times \sin^2\theta] + \langle\alpha_{ii}^2\rangle \times \sin^4\theta \quad (5a)$$

$$I^{\perp}_{SERRS}(\theta) \propto [\Gamma^2(1+\varepsilon) - 1]^2 \times \langle\alpha_{ii}^2\rangle \times [\cos^2\theta \times \sin^2\theta] + \Gamma^2 \times \langle\alpha_{ij}^2\rangle \times [1+\varepsilon \times \sin^2\theta]^2 \quad (5b)$$

For the polarized SERRS intensities at fixed excitation polarization, we obtain

$$I_{SERRS}(\phi)|_{\bar{\theta}=0^\circ} \propto \Gamma^4 \times (1+\varepsilon)^2 \times \langle\alpha_{ii}^2\rangle \times \cos^2\phi + \Gamma^2 \times \langle\alpha_{ij}^2\rangle \times \sin^2\phi \quad (6a)$$

$$I_{SERRS}(\phi)|_{\bar{\theta}=90^\circ} \propto \Gamma^2(1+\varepsilon)^2 \times \langle\alpha_{ij}^2\rangle \times \cos^2(\pi/2-\phi) + \langle\alpha_{ii}^2\rangle \times \sin^2(\pi/2-\phi) \quad (6b)$$

$$I_{SERRS}(\phi)|_{\bar{\theta}=150^\circ} \propto 3/4 \times \Gamma^4(1+\varepsilon)^2 \times \langle\alpha_{ii}^2\rangle \times \cos^2(5\pi/6-\phi) - \sqrt{3}/4 \times \Gamma^2(1+\varepsilon) \times \langle\alpha_{ij}^2\rangle \times \sin(5\pi/3-2\phi) + \Gamma^2 \times \langle\alpha_{ij}^2\rangle \times [\sin\phi + 1/2 \times \varepsilon \times \cos(5\pi/6-\phi)]^2 + 1/4 \times \langle\alpha_{ii}^2\rangle \times \sin^2(5\pi/6-\phi) \quad (6c)$$

For the unpolarized SERRS signal, we have

$$I^{unpol}_{SERRS}(\theta) \propto \Gamma^4(1+\varepsilon)^2 \times \langle\alpha_{ii}^2\rangle \times \cos^2\theta + \Gamma^2 \times \langle\alpha_{ij}^2\rangle \times [1+\varepsilon(2+\varepsilon) \times \sin^2\theta] + \langle\alpha_{ii}^2\rangle \times \sin^2\theta \quad (7)$$

These formulas support the considerations drawn above: (i) the SERRS enhancement factor $\Gamma_{SERRS} = \Gamma^4(1+\varepsilon)^2$ can be exactly calculated as $\Gamma_{SERRS} = I^{\parallel}_{SERRS}|_{\theta=0^\circ}/I^{\parallel}_{SERRS}|_{\theta=90^\circ}$ (eq 5a); (ii) the minima in the cross-polarized signal are not equal since $I^{\perp}_{SERRS}|_{\theta=0^\circ} \neq I^{\perp}_{SERRS}|_{\theta=90^\circ}$ (eq 5b), and the factor $\Delta = I^{\perp}_{SERRS}|_{\theta=90^\circ}/I^{\perp}_{SERRS}|_{\theta=0^\circ} = (1+\varepsilon)^2$ is equal to the ratio between the re-radiation and the excitation FE factors $|\Gamma_{rad}(\lambda_R)|^2/|\Gamma_{exc}(\lambda_L)|^2$. The depolarization ratio is given by $\rho = [(I_{SERRS}|_{\bar{\theta}=0^\circ,\phi=90^\circ} \times I_{SERRS}|_{\bar{\theta}=90^\circ,\phi=90^\circ})/(I_{SERRS}|_{\bar{\theta}=0^\circ,\phi=0^\circ} \times I_{SERRS}|_{\bar{\theta}=90^\circ,\phi=0^\circ})]^{1/2}$ (eqs 6a and 6b). Equations 5−7 correctly yield the classical formulas for polarized Raman scattering[61] in the absence of any enhancement (see Supporting Information, section 3.6).

We have used eqs 5−7 to fit the experimental data (Figures 3−5, solid lines) and estimate the physical parameters of the experiment. We find $|\Gamma_{exc}(\lambda_L)| = 2.4 \pm 0.2$ and $|\Gamma_{rad}(\lambda_R)|/|\Gamma_{exc}(\lambda_L)| = 1.2 \pm 0.1$; that is, the FE factor at the Raman wavelength is about 20% higher with respect to the excitation FE value, in agreement with the transmission measurement information. The errors associated with the calculated parameters (~10%) obtained from the fit, are the physical consequence of the spread in NW diameter and gap size, highlighted in the AFM images of Figure 1a and Supporting Information Figure S1. Indeed, these values have to be considered as average values on ~5−6 NWs/cavities assemblies and not as the enhancement factors of a single nanowire/nanocavity, due to the extension of the laser spot (600 nm diameter) probing several structures at the same time (red spot in Figure 1a). From the fit, we find also the depolarization ratio $\rho = \langle\alpha_{ij}^2\rangle/\langle\alpha_{ii}^2\rangle = 0.55 \pm 0.15$, which is consistent with that found on glass ($\rho \cong 0.5$) and different from the SERRS value on metal NPs ($\rho \cong 1/3$). For instance, eqs 5a and 5b correctly predict that the depolarization ratio of molecules adsorbed on metal NPs, acting as randomly oriented nanocavities, is $\rho = \int_0^{2\pi} I^{\perp}_{SERRS}(\theta)d\theta / \int_0^{2\pi} I^{\parallel}_{SERRS}(\theta)d\theta \approx 1/3$, constant and independent from the Raman polarizability tensor of the molecule,[33] provided that the re-radiation FE factor is $|\Gamma_{rad}(\lambda_R)| \gg 1$.

Some comments on the obtained results are needed. To get information on the relative excitation to re-radiation FE factor, an experimental dynamic range $\sim\Gamma^2$ is necessary, together with a geometrical configuration capable of depleting the Γ^4 term (see eq 5b). An even larger dynamic range, $\sim\Gamma^4$, is necessary for a precise evaluation of the SERRS signal enhancement factor since we must detect the Raman scattering in the absence of any plasmonic enhancement. For nonresonant molecules, this signal falls below the experimental noise threshold.[34,35,41] Choosing probe molecules that can be excited at resonance, as MB or Rhodamine 6G, permits one to take advantage of the resonant Raman amplification and measure the Raman scattering in the absence of SERS enhancement, so to estimate the FE factors without external intensity standards.[32,48,60] A further comment regards the number of molecules actually experiencing SERRS in our experiment. By calculating $\Gamma_{SERRS} \approx 40$, we implicitly assume that the same number of molecules is involved in the RRS (laser and Raman fields parallel to the NWs long axis) and in the SERRS process (laser and Raman fields parallel to the nanocavity axis). This provides a rather conservative estimate of Γ_{SERRS} and can be considered as an average enhancement provided by the whole sample, that is, by the resonant excitation of plasmons localized at both the wire-to-wire nanocavities[46] and along the NWs short axis.[59,60] If we instead assume that the molecules contributing to the polarized SERRS scattering are only the fraction n_c located in the wire-to-wire nanocavities (*ca.* 1/5 of the total molecules n_0 contributing to the RRS signal for our geometry), normalizing to the factor n_c/n_0, we find $\Gamma_{SERRS} \approx 200$.

Our approach to the calculation of the polarized SERRS signals starts from simple EM considerations.[19,21] We assume linear enhancement for both the excitation and the Raman fields and model the anisotropic enhancement of the NWs through the tensors $\overleftrightarrow{\Gamma}_{exc}$ and $\overleftrightarrow{\Gamma}_{rad}$. This leads to eq 3 which shows that in a first approximation the SERS intensity is proportional to $\Gamma_{SERRS} = \Gamma^2_{exc}(\lambda_L) \times \Gamma^2_{rad}(\lambda_R)$. This is the same result coming out from the well-known E^4 model expression, so-called since the total signal enhancement is the product of the square of the excitation FE, $\Gamma_{exc}{}^2(\lambda_L) = |\vec{\mathbf{E}}^{enh}_{exc}|^2/|\vec{\mathbf{E}}_{exc}{}^0|^2$, times the square of the re-radiation FE, $\Gamma^2_{rad}(\lambda_R) = |\vec{\boldsymbol{\mu}}^{enh}_{rad}|^2/|\vec{\boldsymbol{\mu}}^0_{rad}|^2$. Our calculations show that the E^4 expression is only a first approximation since there are terms on the order of $\Gamma_{exc}(\lambda_L) \times \Gamma_{rad}(\lambda_R)$, that is, beyond the E^4 model, that are experimentally relevant and measurable when the term $\sim\Gamma_{exc}{}^2(\lambda_L) \times \Gamma_{rad}{}^2(\lambda_R)$ is geometrically suppressed. The formalism developed in this article can be used to model the SERS response also from asymmetric structures, provided that the enhancement tensors for the specific geometry at the given excitation/Raman wavelengths are known (*e.g.*, by generalized Mie scattering theory calculations[14,15]). In the case of trimers, for example, by using the tensors forms reported in ref 14, we find a general formula for the polarized SERS intensity (see eq S5 in Supporting Information) that, in turn, yields relations equivalent to those found by the authors for both the total intensity and the depolarization factor (eqs S6 and S7). Interestingly, from the comparison between ours and ref 14 calculations, it comes out that assuming tensors in which the nonenhanced elements are strictly "0" (field totally depleted), instead of "1" (field unperturbed), yields only terms on the order $\sim\Gamma_{exc}{}^2(\lambda_L) \times \Gamma_{rad}{}^2(\lambda_R)$ in the expressions of the polarized SERS intensities. This puts forward the relevance of exactly knowing the amplitude of the electromagnetic field at the nanocavity between NPs (dimers or trimers) or between coupled NWs also when the polarization is orthogonal to the nanocavity axis. Finally, we want to stress how the approximation $\Gamma_{SERRS} = |\vec{\mathbf{E}}^{enh}_{exc}|^4/|\vec{\mathbf{E}}^0_{exc}|^4$, based on the assumption that $\Gamma_{exc}(\lambda_L) \cong \Gamma_{rad}(\lambda_R)$ since $|\lambda_R - \lambda_L|/\lambda_L \ll 1$, can lead to misleading predictions. Indeed, the effective excitation field in NWs and NRs is $|\vec{\mathbf{E}}^{enh}_{exc}| \propto \cos\theta$. The straightforward application of the $\Gamma_{SERRS} = |\vec{\mathbf{E}}^{enh}_{exc}|^4/|\vec{\mathbf{E}}^0_{exc}|^4$ approximation yields, however, a misleading SERS dependence as $\cos^4\theta$ since it does not specify to which experimental configuration this law refers to (parallel-polarized, cross-polarized, unpolarized SERS). Equation 4 provides a good first-order approximation of the pSERRS signals. The latter is valid if (i) the excitation and the Raman fields are resonant with the LSPRs, that is, for $|\lambda_{L,R} - \lambda_{LSP}| < \Delta\lambda_{LSP}$, and (ii) the FE factors are large enough to verify the condition $\Gamma^4 \gg \Gamma^2 \gg 1$. In a very general way, we can conclude that whenever the experiments are sensitive to the polarizations of both the excitation and the SERS field, we have to expect a fourth-power dependence of the SERS intensity on the polarization angle (can be $\cos^4\theta$ or $\cos^2\theta \times \sin^2\theta$).[38,41] Conversely, if experiments are sensitive only to either the excitation or the scattered field polarization (as for the unpolarized SERS), an intensity dependence proportional to the square of the FE ($I_{SERS} \propto \cos^2\theta$) should be expected.[35,37,42,59]

CONCLUSIONS

In summary, we have carried out a complete set of polarization-sensitive SERS experiments on randomly oriented MB molecules adsorbed on anisotropic gold NWs. We have experimentally found the correct angular relations for the unpolarized, polarized, and parallel- and cross-polarized SERS intensities. Our experiments highlight the selective enhancement of the Raman dipole component parallel to the nanocavity axis, independently from the excitation field polarization. Assuming linear relations for the enhancement of both the excitation and the Raman fields and introducing a FE tensor to describe the anisotropic properties of the NWs, we develop a model that correctly describes the experimental results for any polarization configuration

and is also capable to predict the polarization behavior of asymmetric structures. Our model yields terms beyond the E^4 approximation, which find full confirmation in the experiment and are key for the independent evaluation of the excitation and re-radiation FE factors. We find that the re-radiation FE factor is 20% stronger with respect to the excitation one, confirming the indications obtained from the extinction profile. Additionally, our analysis provides the depolarization ratio of the C−N−C mode of MB at 446 cm^{-1}, demonstrating that it is possible to gain information on the nondiagonal components of the molecular Raman tensor, provided that an experimental dynamic range $\sim|\Gamma_{exc}|^2$ is achieved. Our analysis suggests that the fields polarizations can be exploited to improve the performances of NW-based SERS sensors to efficiently single out the polarized scattering of molecules bound to the NWs from the unpolarized background signal.

METHODS

Gold Nanowire Preparation by Ion Beam Sputtering. Ion beam sputtering enables the formation of functional nanostrucutred substrates, for example, with tunable chemical reactivity (more information in Supporting Information).[66] SERS-active NW arrays have been produced over large areas in a single maskless step by controlled IBS performed in vacuum conditions (base pressure in the low 10^{-7} mbar range) with the ion beam incident on polycrystalline metal surfaces (Au). A pristine polycrystalline Au film (thickness 150 nm) has been grown by thermal evaporation on standard microscope (soda-lime) glass slides. The flat gold film presents a uniform distribution of connected grains and a dominant population of grains with a diameter peaked around 80 nm. The initial root-mean-square (rms) roughness of the as-deposited film amounts to about 2.3 nm. The Au films present a predominant (111) texture as revealed by X-ray diffraction (XRD) measurements,[67] and in agreement with the findings of other groups.[68,69] The polycrystalline Au sample has been exposed to defocused ion beam sputtering from a gridded multiaperture Ar^+ source (Tectra Instruments). We chose a grazing sputtering angle $\theta = 82°$ measured with respect to the normal and a sputtering energy $E = 800$ eV, while the ion dose was increased at a constant flux of 5.5×10^{14} ions/cm^2 (measured in a plane parallel to the sample surface). The sample temperature is stabilized around $T \sim 300$ K during the sputtering process by means of a cooled sample holder. In order to prevent charge buildup during ion irradiation, electron thermionic emission is ensured from a biased tungsten filament placed in the vicinity of the ion extraction grid.

Atomic Force Microscopy. The morphology of the samples was investigated *ex situ* by means of AFM (Nanosurf Mobile S) operating in intermittent contact mode equipped with ultrasharp Si tips (PPP-NCRL by Nanosensor).

Scanning Electron Microscopy. Structural characterization of the gold nanoparticles was performed by using a field emission scanning electron microscope Zeiss Supra 25.

Absorption and Extinction Spectroscopy. Absorption spectroscopy of MB aqueous solutions was carried out with a Perkin-Elmer Lamda-20 spectrometer. The same instrument was used for extinction measurements, that is, absorption plus scattering, on the gold nanospheres.[70] Polarized extinction measurements on the nanowires were carried out with a fiber-coupled, solid-state spectrometer (Ocean Optics HR4000) using a deuterium halogen lamp (Mikropak, DH-2000-BAL) in the 300−1100 nm range at normal incidence.

Polarization-Sensitive Raman and Surface-Enhanced Raman Spectroscopy. Polarization-sensitive Raman spectroscopy was carried out with a Jobin-Yvon HR800 microspectrometer coupled to a linearly polarized HeNe laser emitting at 633 nm. The excitation power was set between 0.8 and 80 μW. Light was focused on a spot of ~600 nm diameter *via* a 100× microscope objective (NA 0.9). The same objective was used to collect the backscattered radiation. A silicon CCD camera was used for light detection. Typical integration times ranged from 10 to 30 s. A polarization analyzer was mounted on a rotating mount and placed in front of the monochromator slits. Spectral analysis was accomplished with a 600 L/mm grating, featuring a 10% difference in the polarization response to the two transverse electric and transverse magnetic components. A polarization scrambler was used to compensate for such effect.

Theoretical Modeling. To find the polarization dependence of the SERS signal, calculations were carried out in several steps:

1. We define the laboratory reference frame $\{x,y,z\}$ (see Figure S10). In this frame, we assume that the laser excitation propagates along z and the field $\vec{\mathbf{E}}^0_{exc}$ is linearly polarized along the x direction: $\hat{\mathbf{e}}_{exc} \parallel \hat{\mathbf{x}}$.
2. We define the nanowire reference frame $\{x',y',z'\}$ assuming $\hat{\mathbf{x}}' \parallel \hat{\mathbf{n}}_x$, $\hat{\mathbf{y}}' \parallel \hat{\mathbf{n}}_y$, $\hat{\mathbf{z}}' \parallel \hat{\mathbf{z}}$, and call θ the angle between the laser field polarization $\hat{\mathbf{e}}_{exc}$ and the nanocavity direction $\hat{\mathbf{n}}_x$, that is, $\hat{\mathbf{e}}_{exc} \cdot \hat{\mathbf{n}}_x = \hat{x} \cdot x' = \cos\theta$.
3. In the nanowire reference frame $\{x',y',z'\}$ we model the local field enhancement induced by LSP at wavelength λ_L by the tensor

$$\vec{\vec{\Gamma}}_{exc} = \begin{pmatrix} \Gamma & 0 & 0 \\ 0 & 1 & 0 \\ 0 & 0 & 1 \end{pmatrix} \tag{8}$$

This tensor only enhances the laser field component along the nanocavity axis $\hat{\mathbf{n}}_x$ (by a factor Γ), leaving unchanged the orthogonal components. The local enhanced field is therefore given by $\vec{\mathbf{E}}'_{enh} = \vec{\vec{\Gamma}}_{exc} \cdot \vec{\mathbf{E}}'_0$, where $\vec{\mathbf{E}}'_0$ is the incident field calculated in the nanowires reference frame. $\vec{\mathbf{E}}'_0$ is related to $\vec{\mathbf{E}}^0_{exc}$ by a rotation of an angle θ along the z axis through the rotation matrix

$$\vec{\vec{\mathbf{R}}}_z(\theta) = \begin{pmatrix} \cos\theta & \sin\theta & 0 \\ -\sin\theta & \cos\theta & 0 \\ 0 & 0 & 1 \end{pmatrix} \tag{9}$$

4. In the nanowire reference frame, we define the generic Raman polarizability tensor

$$\vec{\vec{\alpha}} = \begin{pmatrix} \alpha_{xx} & \alpha_{xy} & \alpha_{xz} \\ \alpha_{yx} & \alpha_{yy} & \alpha_{yz} \\ \alpha_{zx} & \alpha_{zy} & \alpha_{zz} \end{pmatrix} \tag{10}$$

for a given Raman mode of a molecule having a generic spatial orientation. We do not make any assumption on the symmetry of the molecule, that is, on the specific form of the tensor. The Raman-induced dipole will be $\vec{\boldsymbol{\mu}}' = \vec{\vec{\alpha}} \cdot \vec{\mathbf{E}}'_{enh}$. Differently oriented molecules feature a Raman polarizability tensor whose components transform as $\alpha'_{ij} = R_{ik}(\xi,\zeta,\psi)R_{jl}(\xi,\zeta,\psi)\alpha_{kl}$, where we have adopted Einstein's sum rule on the repeated indices and where

$$R(\phi,\theta,\psi) = \begin{pmatrix} \cos\psi & \sin\psi & 0 \\ -\sin\psi & \cos\psi & 0 \\ 0 & 0 & 1 \end{pmatrix} \begin{pmatrix} 1 & 0 & 0 \\ 0 & \cos\zeta & \sin\zeta \\ 0 & -\sin\zeta & \cos\zeta \end{pmatrix} \begin{pmatrix} \cos\xi & \sin\xi & 0 \\ -\sin\xi & \cos\xi & 0 \\ 0 & 0 & 1 \end{pmatrix} \tag{11}$$

is the rotation matrix associated with Euler angles (ξ,ζ,ψ) of the molecule in the considered reference frame.

5. In the nanowire reference frame, we model the re-radiation enhancement by the tensor

$$\vec{\vec{\Gamma}}_{rad} = \begin{pmatrix} \Gamma(1+\varepsilon) & 0 & 0 \\ 0 & 1 & 0 \\ 0 & 0 & 1 \end{pmatrix} \quad (12)$$

This tensor enhances only the component of the Raman-induced dipole parallel to the nanocavity axis, by a factor $\Gamma(1 + \varepsilon)$. The factor $(1 + \varepsilon)$ allows us to account for different enhancement factors at λ_R and λ_L. The enhanced Raman dipole will be given by $\vec{\boldsymbol{\mu}}'_{enh} = \vec{\vec{\Gamma}}_{rad} \cdot \vec{\boldsymbol{\mu}}'$.

6. In the laboratory reference frame, we collect the back scattered radiation propagating along $-\hat{\mathbf{z}}$ and analyze the polarization state of the SERS radiation with a polaroid whose optical axis $\hat{\mathbf{e}}_{det}$ is rotated at an angle ϕ with respect to the laser pump field ($\hat{\mathbf{e}}_{det} \cdot \hat{\mathbf{x}} = \cos\theta$). For a single molecule, we will therefore have $I_{SERS}(\theta,\phi) = |\vec{\boldsymbol{\mu}}_{enh} \cdot \hat{\mathbf{e}}_{det}|^2$, where $\vec{\boldsymbol{\mu}}_{enh}$ is the enhanced Raman dipole calculated in the laboratory frame, related to $\vec{\boldsymbol{\mu}}'_{enh}$ by a rotation $\mathbf{R}_z(-\theta)$ around the z axis.

7. For many randomly oriented molecules, the calculation of the SERS intensity is carried out by exploiting the incoherent nature of the Raman scattering; that is, the phase Raman fields scattered by different molecules are random. Consequently, the total signal can be considered as the sum of the emission from any single molecule, that is

$$I_{SERS}(\theta,\phi) = \left| \sum_{i=1\ldots N} \vec{\boldsymbol{\mu}}^{(i)}_{enh} \cdot \hat{\mathbf{e}}_{det} \right|^2 = \sum_{i=1\ldots N} \left| \vec{\boldsymbol{\mu}}^{(i)}_{enh} \cdot \hat{\mathbf{e}}_{det} \right|^2 \quad (13)$$

This, in turn, will be given by the number of molecules in the cavity times the angular averaged Raman emission of a single molecule, that is

$$\begin{aligned} I_{SERS}(\theta,\phi) &= n_c \cdot \langle |\vec{\mu}_{enh} \cdot \hat{\mathbf{e}}_{det}|^2 \rangle_{\xi,\zeta,\psi} \\ &= n_c \cdot \langle |\hat{\mathbf{e}}_{det} \cdot \vec{\vec{\mathbf{R}}}_z(-\theta) \cdot \vec{\vec{\Gamma}}_{rad}(\lambda_R) \cdot \vec{\vec{\alpha}}(\xi,\zeta,\psi) \cdot \vec{\vec{\Gamma}}_{exc}(\lambda_L) \\ &\quad \cdot \vec{\vec{\mathbf{R}}}_z(\theta) \cdot \hat{\mathbf{e}}_{exc}|^2 \rangle_{\xi,\zeta,\psi} \end{aligned} \quad (14)$$

that can be calculated as

$$I_{SERS}(\theta,\phi) = \int_0^{2\pi} d\psi \int_0^{\pi} \sin\zeta d\zeta \int_0^{2\pi} d\xi |\hat{\mathbf{e}}_{det} \cdot \vec{\vec{\mathbf{R}}}_z(-\theta) \cdot \vec{\vec{\Gamma}}_{rad}(\lambda_R) \cdot \vec{\vec{\alpha}}(\xi,\zeta,\psi) \cdot \vec{\vec{\Gamma}}_{exc}(\lambda_L) \cdot \vec{\vec{\mathbf{R}}}_z(\theta) \cdot \hat{\mathbf{e}}_{exc}|^2 \quad (15)$$

8. Calculations are simplified accounting for the following identity relations among the angular averages of the tensor components:[61] $\langle \alpha_{xx}^2 \rangle = \langle \alpha_{yy}^2 \rangle$, $\langle \alpha_{xy}^2 \rangle = \langle \alpha_{yx}^2 \rangle$, $\langle \alpha_{xx} \cdot \alpha_{xy} \rangle = \langle \alpha_{xx} \cdot \alpha_{yx} \rangle = 0$, $\langle \alpha_{xy} \cdot \alpha_{yy} \rangle = \langle \alpha_{yx} \cdot \alpha_{yy} \rangle = 0$, $\langle \alpha_{xy} \cdot \alpha_{yx} \rangle + \langle \alpha_{xx} \cdot \alpha_{yy} \rangle = \langle \alpha_{xx}^2 \rangle - \langle \alpha_{xy}^2 \rangle$. Since we are working in a backscattering configuration, the z-components of the Raman polarizability tensor do not figure in the equations.

Acknowledgment. We acknowledge support by MIUR under Project PRIN 2008J858Y7. B.F., C.D'A., and P.G.G. acknowledge funding from the European Union Seventh Framework Programme (FP7/2007-2013) under Grant Agreement No. 241818 (FP7-HEALTH-F5-2009-241818-NANOANTENNA). F.B.dM. acknowledges support by CNISM under project Innesco, by MAE under program Italia-Polonia, by Fondazione CARIGE and by ENEA under contract MSE.

Supporting Information Available: Advantages of ion beam sputtering, AFM images, Methylene Blue molecules (preparation description and characterization: UV−vis absorption spectrum, polarized RRS), morphology, extinction, and polarized SERRS from gold nanoparticles, polar plots of polarized SERRS from NWs, depolarization factor from randomly oriented molecules, checks on theoretical mode, theoretical calculations on trimers. This material is available free of charge *via* the Internet at http://pubs.acs.org.

REFERENCES AND NOTES

1. Mühlschlegel, P.; Eisler, H.-J.; Martin, O. J. F.; Hecht, B.; Pohl, D. W. Resonant Optical Nanoantennas. *Science* **2005**, *308*, 1607–1609.
2. Taminiau, T. H.; Moerland, R. J.; Segerink, F. B.; Kuipers, L.; van Hulst, N. F. $\lambda/4$ Resonance of an Optical Monopole Antenna Probed by Single Molecule Fluorescence. *Nano Lett.* **2007**, *7*, 28–33.
3. Hartschuh, A.; Sánchez, E.; Xie, X.; Novotny, L. High-Resolution Near-Field Raman Microscopy of Single-Walled Carbon Nanotubes. *Phys. Rev. Lett.* **2003**, *90*, 7–10.
4. Bozhevolnyi, S. I.; Volkov, V. S.; Devaux, E.; Laluet, J. Y.; Ebbesen, T. W. Channel Plasmon Subwavelength Waveguide Components Including Interferometers and Ring Resonators. *Nature* **2006**, *440*, 508–511.
5. Gramotnev, D. K.; Bozhevolnyi, S. I. Plasmonics beyond the Diffraction Limit. *Nat. Photonics* **2010**, *4*, 83–91.
6. Fang, Y.; Li, Z.; Huang, Y.; Zhang, S.; Nordlander, P.; Halas, N. J.; Xu, H. X. Branched Silver Nanowires as Controllable Plasmon Routers. *Nano Lett.* **2010**, *10*, 1950–1954.
7. Neubrech, F.; Pucci, A.; Cornelius, T. W.; Karim, S.; Garcia-Etxarri, A.; Aizpurua, J. Resonant Plasmonic and Vibrational Coupling in a Tailored Nanoantenna for Infrared Detection. *Phys. Rev. Lett.* **2008**, *101*, 157403.
8. Ming, T.; Zhao, L.; Yang, Z.; Chen, H.; Sun, L.; Wang, J.; Yan, C. Strong Polarization Dependence of Plasmon-Enhanced Fluorescence on Single Gold Nanorods. *Nano Lett.* **2009**, *9*, 3896–3903.
9. Farahani, J. N.; Pohl, D. W.; Eisler, H. J.; Hecht, B. Single Quantum Dot Coupled to a Scanning Optical Antenna: A Tunable Superemitter. *Phys. Rev. Lett.* **2005**, *95*, 017402.
10. Moskovitz, M. Surface-Enhanced Spectroscopy. *Rev. Mod. Phys.* **1985**, *57*, 783–826.
11. Kneipp, K.; Moskovits, M.; Kneipp, H. *Surface Enhanced Raman Scattering*; Springer: New York, 2006.
12. Le Ru, E.; Etchegoin, P. *Principles of Surface Enhanced Raman Spectroscopy*; Elsevier: Amsterdam, 2009.
13. Li, Z.; Bao, K.; Fang, Y.; Nordlander, P.; Xu, H. X. Correlation between Incident and Emission Polarization in Nanowire Surface Plasmon Waveguides. *Nano Lett.* **2010**, *10*, 1831–1835.
14. Shegai, T.; Li, Z.; Dadosh, T.; Zhang, Z.; Xu, H.; Haran, G. Managing Light Polarization *via* Plasmon−Molecule Interactions within an Asymmetric Metal Nanoparticle Trimer. *Proc. Natl. Acad. Sci. U.S.A.* **2008**, *105*, 16448–16453.
15. Li, Z. P.; Shegai, T.; Haran, G.; Xu, H. X. Multiple-Particle Nanoantennas for Enormous Enhancement and Polarization Control of Light Emission. *ACS Nano* **2009**, *3*, 637–642.
16. Taminiau, T. H.; Stefani, F. D.; Segerink, F. B.; van Hulst, N. F. Optical Antennas Direct Single-Molecule Emission. *Nat. Photonics* **2008**, *2*, 234–237.
17. Curto, A. G.; Volpe, G.; Taminiau, T. H.; Kreuzer, M. P.; Quidant, R.; van Hulst, N. F. Unidirectional Emission of a Quantum Dot Coupled to a Nanoantenna. *Science* **2010**, *329*, 930–933.
18. Li, Z. P.; Hao, F.; Huang, Y. Z.; Fang, Y. R.; Nordlander, P.; Xu, H. X. Directional Light Emission from Propagating Surface Plasmons of Silver Nanowires. *Nano Lett.* **2009**, *9*, 4383–4386.
19. Lee, S. J.; Guan, Z.; Xu, H.; Moskovits, M. Surface-Enhanced Raman Spectroscopy and Nanogeometry: The Plasmonic Origin of SERS. *J. Phys. Chem. C* **2007**, *11*, 17985–17988.
20. Schatz, G. C.; Young, M. A.; Van Duyne, R. P. Electromagnetic Mechanism of SERS. *Top. Appl. Phys.* **2006**, *103*, 19–45.
21. Wokaun, A. Surface-Enhanced Electromagnetic Processes. *Solid State Phys.* **1984**, *38*, 223–294.

22. Hao, E.; Schatz, G. C. Electromagnetic Fields Around Silver Nanoparticles and Dimers. *J. Chem. Phys.* **2004**, *120*, 357–366.
23. Schnell, M.; Garcia-Etxarri, A.; Huber, A. J.; Crozier, K.; Alkorta, J.; Aizpurua, J.; Hillenbrand, R. Controlling the Near-Field Oscillations of Loaded Plasmonic Nanoantennas. *Nat. Photonics* **2009**, *3*, 287–291.
24. Schnell, M.; Garcia-Etxarri, A.; Alkorta, J.; Aizpurua, J.; Hillenbrand, R. Phase-Resolved Mapping of the Near-Field Vector and Polarization State in Nanoscale Antenna Gaps. *Nano Lett.* **2010**, *10*, 3524–3528.
25. Quin, L.; Zou, S.; Xue, C.; Atkinson, A.; Schatz, G. C.; Mirkin, C. A. Designing, Fabricating, and Imaging Raman Hot Spots. *Proc. Natl. Acad. Sci. U.S.A.* **2006**, *103*, 13300–13303.
26. Garcia-Vidal, F. J.; Pendry, J. B. Collective Theory for Surface Enhanced Raman Scattering. *Phys. Rev. Lett.* **1996**, *77*, 1163–1166.
27. Gucciardi, P. G.; Lopes, M.; Déturche, R.; Julien, C.; Barchiesi, D.; Lamy de la Chapelle, M. Light Depolarization Induced by Metallic Tips in Apertureless Near-Field Optical Microscopy and Tip-Enhanced Raman Spectroscopy. *Nanotechnology* **2008**, *19*, 215702.
28. Gucciardi, P.; Bonaccorso, F.; Lopes, M.; Billot, L.; De La Chapelle, M. Light Depolarization Induced by Sharp Metallic Tips and Effects on Tip-Enhanced Raman Spectroscopy. *Thin Solid Films* **2008**, *516*, 8064–8072.
29. Merlen, A.; Valmalette, J.-C.; Gucciardi, P. G.; Lamy del la Chapelle, M.; Frigout, A.; Ossikovski, R. Depolarization Effects in Tip-Enhanced Raman Spectroscopy. *J. Raman Spectrosc.* **2009**, *40*, 1361–1370.
30. Le Ru, E.; Etchegoin, P. Rigorous Justification of the $|E|^4$ Enhancement Factor in Surface Enhanced Raman Spectroscopy. *Chem. Phys. Lett.* **2006**, *423*, 63–66.
31. Nagasawa, F.; Takase, M.; Nabika, H.; Murakishi, K. Polarization Characteristics of Surface-Enhanced Raman Scattering from a Small Number of Molecules at the Gap of a Metal Nano-Dimer. *Chem. Commun.* **2011**, *47*, 4514–4516.
32. Le Ru, E. C.; Grand, J.; Félidj, N.; Aubard, J.; Lévi, G.; Hohenau, a; Krenn, J. R.; Blackie, E.; Etchegoin, P. G. Experimental Verification of the SERS Electromagnetic Model beyond the $|E|^4$ Approximation: Polarization Effects. *J. Phys. Chem. C* **2008**, *112*, 8117–8121.
33. Le Ru, E. C.; Meyer, M.; Blackie, E.; Etchegoin, P. G. Advanced Aspects of Electromagnetic SERS Enhancement Factors at a Hot Spot. *J. Raman Spectrosc.* **2008**, *39*, 1127–1134.
34. Nie, S. M.; Emory, S. R. Probing Single Molecules and Single Nanoparticles by Surface-Enhanced Raman Scattering. *Science* **1997**, *275*, 1102–1106.
35. Grand, J.; De La Chapelle, M. L.; Bijeon, J.-L.; Adam, P.-M.; Vial, A.; Royer, P. Role of Localized Surface Plasmons in Surface-Enhanced Raman Scattering of Shape-Controlled Metallic Particles in Regular Arrays. *Phys. Rev. B* **2005**, *73*, 033407.
36. Baik, J. M.; Lee, S. J.; Moskovits, M. Polarized Surface-Enhanced Raman Spectroscopy from Molecules Adsorbed in Nano-Gaps Produced by Electromigration in Silver Nanowires. *Nano Lett.* **2009**, *9*, 672–679.
37. Wei, H.; Hao, F.; Huang, Y.; Wang, W.; Nordlander, P.; Xu, H. X. Polarization Dependence of Surface-Enhanced Raman Scattering in Gold Nanoparticle-Nanowire Systems. *Nano Lett.* **2008**, *8*, 2497–2502.
38. Etchegoin, P. G.; Galloway, C.; Le Ru, E. C. Polarization-Dependent Effects in Surface-Enhanced Raman Scattering (SERS). *Phys. Chem. Chem. Phys.* **2006**, *8*, 2624–2628.
39. Bosnick, K. A.; Jiang, J.; Brus, L. E. Fluctuations and Local Symmetry in Single-Molecule Rhodamine 6G Raman Scattering on Silver Nanocrystal Aggregates. *J. Phys. Chem. B* **2002**, *106*, 8096–8099.
40. Jiang, J.; Bosnick, K. A.; Maillard, M.; Brus, L. E. Single Molecule Raman Spectroscopy at the Junctions of Large Ag Nanocrystals. *J. Phys. Chem. B* **2003**, *107*, 9964–9972.
41. Xu, H. X.; Käll, M. Polarization-Dependent Surface-Enhanced Raman Spectroscopy of Isolated Silver Nanoaggregates. *ChemPhysChem* **2003**, *4*, 1001–1005.
42. Brolo, A. G.; Arctander, E.; Addison, C. J. Strong Polarized Enhanced Raman Scattering *via* Optical Tunneling through Random Parallel Nanostructures in Au Thin Films. *J. Phys. Chem. B* **2005**, *109*, 401–405.
43. Tao, A. R.; Yang, P. Polarized Surface-Enhanced Raman Spectroscopy on Coupled Metallic Nanowires. *J. Phys. Chem. B* **2005**, *109*, 15687–15690.
44. Zhao, Y.-P.; Chaney, S. B.; Shanmukh, S.; Dluhy, R. A. Polarized Surface Enhanced Raman and Absorbance Spectra of Aligned Silver Nanorod Arrays. *J. Phys. Chem. B* **2006**, *110*, 3153–3157.
45. Liu, Y.; Fan, J.; Zhao, Y. −P.; Shanmukh, S.; Dluhy, R. A. Angle Dependent Surface Enhanced Raman Scattering Obtained from a Ag Nanorod Array Substrate. *Appl. Phys. Lett.* **2006**, *89*, 173134.
46. Jeong, D. H.; Zhang, Y. X.; Moskovits, M. Polarized Surface Enhanced Raman Scattering from Aligned Silver Nanowire Rafts. *J. Phys. Chem. B* **2004**, *108*, 12724–12728.
47. Shegai, T. O.; Haran, G. Probing the Raman Scattering Tensors of Individual Molecules. *J. Phys. Chem. B* **2006**, *110*, 2459–24561.
48. McFarland, A. D.; Young, M.; Dieringer, J.; Van Duyne, R. P. Wavelength-Scanned Surface-Enhanced Raman Excitation Spectroscopy. *J. Phys. Chem. B* **2005**, *109*, 11279–11285.
49. Le Ru, E. C.; Etchegoin, P. G.; Grand, J.; Felidj, N.; Aubard, J.; Levi, G.; Hohenau, A.; Krenn, J. R. Surface Enhanced Raman Spectroscopy on Nanolithography-Prepared Substrates. *Curr. Appl. Phys.* **2008**, *8*, 467–470.
50. Schedin, F.; Lidorikis, E.; Lombardo, A.; Kravets, V. G.; Geim, A. K.; Grigorenko, A. N.; Novoselov, K. S.; Ferrari, A. C. Surface-Enhanced Raman Spectroscopy of Graphene. *ACS Nano* **2010**, *4*, 5617–5626.
51. Billot, L.; Lamy de La Chapelle, M.; Grimault, A.; Vial, A.; Barchiesi, D.; Bijeon, J.; Adam, P.; Royer, P. Surface Enhanced Raman Scattering on Gold Nanowire Arrays: Evidence of Strong Multipolar Surface Plasmon Resonance Enhancement. *Chem. Phys. Lett.* **2006**, *422*, 303–307.
52. Luk'yanchuk, B.; Zheludev, N. I.; Mayer, S. A.; Halas, N. J.; Nordlander, P.; Giessen, H.; Chong, C. T. The Fano Resonance in Plasmonic Nanostructures and Metamaterials. *Nat. Mater.* **2010**, *7*, 707–715.
53. Guillot, N.; Shen, H.; Fremaux, B.; Péron, O.; Rinnert, E.; Toury, T.; Lamy de la Chapelle, M. Surface Enhanced Raman Scattering Optimization of Gold Nanocylinder Arrays: Influence of the Localized Surface Plasmon Resonance and Excitation Wavelength. *Appl. Phys. Lett.* **2010**, *97*, 023113.
54. Shanmukh, S.; Jones, L.; Driskell, J.; Zhao, Y.; Dluhy, R.; Tripp, R. Rapid and Sensitive Detection of Respiratory Virus Molecular Signatures Using a Silver Nanorod Array SERS Substrate. *Nano Lett.* **2006**, *6*, 2630–2636.
55. Anema, J. R.; Brolo, A. G. The Use of Polarization-Dependent SERS from Scratched Gold Films To Selectively Eliminate Solution-Phase Interference. *Plasmonics* **2007**, *2*, 157–162.
56. Valbusa, U.; Boragno, C.; de Mongeot, F. B. Nanostructuring by Ion Beam. *Mater. Sci. Eng. C* **2003**, *23*, 201–209.
57. Toma, A.; Chiappe, D.; Šetina Batič, B.; Godec, M.; Jenko, M.; Buatier De Mongeot, F. Erosive *versus* Shadowing Instabilities in the Self-Organized Ion Patterning of Polycrystalline Metal Films. *Phys. Rev. B* **2008**, *78*, 153406.
58. Toma, A.; Chiappe, D.; Boragno, C.; de Mongeot, F. B. Self-Organized Ion-Beam Synthesis of Nanowires with Broadband Plasmonic Functionality. *Phys. Rev. B* **2010**, *81*, 165436.
59. Mohanty, P.; Yoon, I.; Kang, T.; Seo, K.; Varadwaj, K. S. K.; Choi, W.; Park, Q.-H.; Ahn, J. P.; Suh, Y. D.; Ihee, H.; *et al.* Simple Vapor-Phase Synthesis of Single-Crystalline Ag Nanowires and Single-Nanowire Surface-Enhanced Raman Scattering. *J. Am. Chem. Soc.* **2007**, *129*, 9576–9577.
60. Laurent, G.; Félidj, N.; Aubard, J.; Lévi, G.; Krenn, J.; Hohenau, A; Schider, G.; Leitner, A.; Aussenegg, F. Evidence of Multipolar Excitations in Surface Enhanced Raman Scattering. *Phys. Rev. B* **2005**, *71*, 045430.

61. Long, D. *The Raman E□ect*; Wiley: New York, 2002.
62. Tognalli, N. G.; Fainstein, A.; Vericat, C .; Vela, M. E.; Salvarezza, R. C. Exploring Three-Dimensional Nanosystems with Raman Spectroscopy: Methylene Blue Adsorbed on Thiol and Sulfur Monolayers on Gold. *J. Phys. Chem. B* **2006**, *110*, 354–360.
63. Nicolai, S. H. A.; Rubim, J. C. Surface-Enhanced Resonance Raman (SERR) Spectra of Methylene Blue Adsorbed on a Silver Electrode. *Langmuir* **2003**, *19*, 4291–4294.
64. Mahajan, S.; Cole, R. M.; Speed, J. D.; Pelfrey, S. H.; Russell, A. E.; Bartlett, P. N.; Barnett, S. M.; Baumberg, J. J. Understanding the Surface-Enhanced Raman Spectroscopy "Background". *J. Phys. Chem. C* **2010**, *114*, 7242–7250.
65. Turrell, G. Analysis of Polarization Measurements in Raman Microspectroscopy. *J. Raman Spectrosc.* **1984**, *15*, 103–108.
66. de Mongeot, F. B.; Toma, A.; Molle, A.; Lizzit, S.; Petaccia, L.; Baraldi, A. Carbon Monoxide Dissociation on Rh Nanopyramids. *Phys. Rev. Lett.* **2006**, *97*, 056103.
67. Toma, A.; Chiappe, D.; Šetina Batič, B.; Godec, M.; Boragno, C.; Valbusa, U.; Jenko, M.; de Mongeot, F. B. Patterning Polycrystalline Thin Films by Defocused Ion Beam: The Influence of Initial Morphology on the Evolution of Self-Organized Nanostructures. *J. Appl. Phys.* **2008**, *104*, 104313.
68. Rost, M. J.; Quist, D. A.; Frenken, J. W. M. Grains, Growth, and Grooving. *Phys. Rev. Lett.* **2003**, *91*, 026101.
69. Polop, C.; Rosiepen, C.; Bleikamp, S.; Drese, R.; Mayer, J.; Dimyati, A.; Michely, T. The STM View of the Initial Stages of Polycrystalline Ag Film Formation. *New J. Phys.* **2007**, *9*, 74.
70. On metal nanostructures, we speak about extinction rather than absorption spectroscopy since scattering is non-negligible.